MASTER COPY: PLEASE KEEP THIS "MEMORANDUM OF TRANSMITTAL" BLANK FOR REPRODUCTION PURPOSES. WHEN REPORTS ARE GENERATED UNDER THE ARO SPONSORSHIP, FORWARD A COMPLETED COPY OF THIS FORM WITH EACH REPORT SHIPMENT TO THE ARO. THIS WILL ASSURE PROPER IDENTIFICATION. NOT TO BE USED FOR INTERIM PROGRESS REPORTS; SEE PAGE 2 FOR INTERIM PROGRESS REPORT INSTRUCTIONS.

MEMORANDUM OF TRANSMITTAL

U.S. Army Research Office
ATTN: AMSRL-RO-BI (TR)
P.O. Box 12211
Research Triangle Park, NC 27709-2211

☒ Reprint (Orig + 2 copies)
☐ Technical Report (Orig + 2 copies)
☐ Manuscript (1 copy)
☐ Final Progress Report (Orig + 2 copies)
☐ Related Materials, Abstracts, Theses (1 copy)

CONTRACT/GRANT NUMBER: DAA-19-01-1-0638

REPORT TITLE: FADING CHANNELS

is forwarded for your information.

SUBMITTED FOR PUBLICATION TO (applicable only if report is manuscript):
Wiley Encyclopedia of Telecommunications

Sincerely,

Alexandra Duel-Hallen

FADING CHANNELS

Alexandra Duel-Hallen

ECE Department, North Carolina State University.

Keywords: Fading Multipath Channels, Radio Communications, Mobile Radio, Diversity Combining, Multipath Propagation.

Abstract

Fading multipath channels are encountered in many wireless communication systems, including traditional radio communications and modern cellular and personal communication (PCS) mobile radio channels. This paper addresses characterization and modeling of fading channels. Performance issues and mitigation of fading using diversity techniques are also presented.

1. Introduction.

Radio communication channels include shortwave ionospheric radio communication in the 3-30 MHz frequency band (HF), tropospheric scatter (beyond-the-horizon) radio communications in the 300-3000 MHz frequency band (UHF) and 3000-30,000 MHz frequency band (SHF), and ionospheric forward scatter in the 30-300 MHz frequency band (VHF) [1,2]. These channels usually exhibit *multipath propagation* that results from *reflection, diffraction* and *scattering* of the transmitted signal. Multipath propagation and *Doppler effects* due to the motion of the transmitter and/or receiver give rise to *multipath fading* channel characterization. The fading signal is characterized in terms of *large-scale* and *small-scale* fading.

The large-scale fading model describes the average received signal power as a function of the distance between the transmitter and the receiver. Statistical variation

around this mean (on the order of 6-10dB) resulting from shadowing of the signal due to large obstructions is also included in the model of large-scale fading. Large scale fading describes the variation of the received power over large areas and is useful in estimating radio coverage of the transmitter. The large scale fading model is determined by averaging the received power over many wavelengths (e.g., 1-10 meters for cellular and PCS frequencies of 1-2 GHz)[3].

The small-scale fading model describes the instantaneous variation of the received power over a few wavelengths. This variation can result in dramatic loss of power on the order of 40dB. It is due to superposition of several reflected or scattered components coming from different directions. Figure 1 depicts small-scale fading and slower large-scale fading for a mobile radio communication system. The figure illustrates that small-scale variation is averaged out in the large-scale fading model.

In Section 2, we review the large scale fading models. Sections 3-5 describe small scale fading. Multipath fading channels are characterized in Section 3. Section 4 contains useful fading models. Performance analysis for flat fading channels and diversity combining approaches are descried in Section 5.

2. Large-Scale Fading

Propagation path loss $L_s(d)$ is defined as the ratio of the transmitted power to the received power in an radio frequency (RF) channel. In a free space model, the propagation path loss is proportional to d^2, where d is the distance between the transmitter and the receiver. When the receiving antenna is isotropic, this loss is given by [2]:

$$L_s(d) = (4 \pi d / \lambda)^2, \quad (1)$$

where λ is the wavelength of the RF signal. In the mobile radio channel, the average path loss is usually more severe due to obstructions and is inversely proportional to d^n, where $2 \le n \le 6$. The average path loss is given by [2,3]:

$$L_{av}\,(d)\,(dB) = L_s(d_0) + 10n\log_{10}(d/d_0), \qquad (2)$$

where d_0 is the close-in reference distance. This distance corresponds to a point located in the far-field of the antenna. For large cells, it is usually assumed to be 1 km, whereas for smaller cells and indoor environments, the values of 100 m and 1 m, respectively, are used. The value of the exponent n depends on the frequency, antenna heights and the propagation conditions. For example, in urban area cellular radio, n takes on values from 2.7 to 3.5, in building line-of-sight conditions result in $1.6 \le n \le 1.8$, whereas obstructed in building environment corresponds to n from 4 to 6 [3].

The actual path loss in a particular location can significantly deviate from its average value (2) due to *shadowing* of the signal by large obstructions. Measurements show that this variation is approximately *log-normally* distributed. Thus, the path loss is represented by the random variable

$$L_p\,(d)\,(dB) = L_{av}\,(d)\,(dB) + X_\sigma, \qquad (3)$$

where X_σ has Gaussian distribution (when expressed in decibels) with mean zero and standard deviation σ (also in dB). Note that average path loss (2) corresponds to a straight line with slope 10n (dB) per decade when plotted on log-log scale. Thus, in practice, the values of n and σ are determined using linear regression to minimize the difference between the actual measurements (over various locations and distances between the transmitter and receiver) and the estimated average path loss in the mean

squared-error (MSE) sense. Figure 2 illustrates the actual measured data and the estimated average path loss for several transmitter-receiver separation values.

References [1-7] describe appropriate models and approaches to measurement and estimation of propagation path loss for various wireless channels and provide additional useful references on this subject. The rest of this paper is devoted to characterization, modeling and performance analysis of small-scale fading.

3. Characterization of Fading Multipath Channels.

A signal transmitted through a wireless channel arrives at its destination along a number of different paths (referred to as *multipath propagation*) as illustrated in Figure 3. Multipath causes interference between *reflected or scattered* transmitter signal components. As the receiver moves through this *interference pattern*, a typical fading signal results as illustrated in Figure 4. If an unmodulated carrier at the frequency f_c is transmitted over a fading channel, the complex envelope (the *equivalent lowpass signal*) [1] of the received fading signal is given by

$$c(t) = \sum_{n=1}^{N} A_n \, e^{j(2\pi f_n t + 2\pi f_c \tau_n + \phi_n)}, \tag{4}$$

where N is the number of scatterers, and for the n^{th} scatterer, A_n is the *amplitude*, f_n is the *Doppler frequency shift*, τ_n is the *excess propagation delay* (relative to the arrival of the first path) and ϕ_n is the phase. The *Doppler frequency shift* is given by [3]:

$$f_n = f_c \frac{v}{c} \cos\theta = f_{dm} \cos\theta \tag{5}$$

where v is the vehicle speed (assumed constant), c is the speed of light, θ is the incident radio wave angle with respect to the motion of the mobile, and f_{dm} is the *maximum Doppler frequency shift*.

The parameters A_n, f_n, τ_n, and ϕ_n are very *slowly time-variant,* and can be viewed as fixed on the time scale of a few milliseconds. Thus, the signal in (4) is a superposition of complex sinusoids with approximately constant amplitudes, frequencies and phases, and varies in time as the mobile moves through the interference pattern. The superposition of terms in (4) that can result in destructive or constructive interference, causing deep fades or peaks in the received signal, respectively, as illustrated in Figure 4. The power of the fading signal can change dramatically by as much as 30-40dB. This variation can be conveniently modeled by characterizing c(t) as a *stationary random process*. This statistical characterization is useful for describing time dispersion and fading rapidity of multipath fading channels [1-9].

Statistical Characterization

If we assume that the complex envelope of the transmitted signal is $s_l(t)$, the equivalent baseband signal received at the output of the fading channel is:

$$r(t) = \int_{-\infty}^{\infty} c(\tau, t)\, s_l(t-\tau)\, d\tau, \qquad (6)$$

where the time-variant impulse response $c(\tau, t)$ is the response of the channel at time t to the impulse applied at time $t-\tau$ [1]. (In practice, additive Gaussian noise is also present at the output of the channel.) The expression (6) can be viewed as the superposition of delayed and attenuated copies of the transmitted signal $s_l(t)$, where the delays are given by τ_n and the corresponding complex gains have amplitudes A_n (see (4)) and time-variant phases (determined from the phase terms in (4)).

For each delay τ, the response $c(\tau,t)$ is modeled as a *wide sense stationary* stochastic process. Typically, the random processes $c(\tau_1, t)$ and $c(\tau_2, t)$ are uncorrelated for $\tau_1 \neq \tau_2$ since different multipath components contribute to these signals (this is called

uncorrelated scattering). For fixed delay τ, the autocorrelation function of the impulse response is defined as [1]:

$$\phi_c(\tau; \Delta t) = 1/2\ E[c^*(\tau, t)\ c(\tau, t+\Delta t)] \tag{7}$$

The power of $c(\tau, t)$ as a function of the delay τ is

$$\phi_c(\tau; 0) \equiv \phi_c(\tau)\ . \tag{8}$$

It is called *multipath intensity profile* or *power delay profile* and is determined from measurements [1,3]. A "worst case" multipath intensity profile for an urban channel is shown in Figure 5. The range of values of τ where $\phi_c(\tau)$ is non-negligible is called the *multipath spread* of the channel and denoted as T_m. The values of multipath spread vary greatly depending on the terrain. For urban and suburban areas, typical values of multipath spread are from one to ten microseconds, whereas in rural mountainous area, the multipath spreads are much greater with values from 10 to 30 microseconds [1]. The *mean excess delay* and *rms delay spread* σ_τ are defined as the mean and the standard deviation of the excess delay, respectively, and can be determined from the multipath intensity profile [2,3]. Typical rms delay spreads are on the order of one microsecond for urban outdoor channels, hundreds of nanoseconds for suburban channels, and tens of nanoseconds for indoor channels [3].

The Fourier transform of the channel response $c(\tau, t)$ is the time-variant channel transfer function $C(f;t)$. It is also modeled as a wide-sense stationary random process. The correlation

$$\phi_c(\Delta f; \Delta t) = 1/2\ E[C^*(f; t)\ C(f+\Delta f; t+\Delta t)] \tag{9}$$

is called the *spaced-frequency spaced-time autocorrelation function*. It is the Fourier transform of the autocorrelation function $\phi_c(\tau; \Delta t)$ in (7) [1]. It can be shown that this function can be factored into a product of time-domain and frequency-domain correlation functions. The latter is the *spaced-frequency correlation function* $\phi_c(\Delta f;0) \equiv \phi_c(\Delta f)$ and is the Fourier transform of the multipath intensity profile $\phi_c(\tau)$ in (8) [1].

The complex envelope of the response C(f;t) is specified by (4) with f viewed as the frequency of the unmodulated input carrier. Consider input frequency separation Δf. In the expressions for C(f;t) and C(f+Δf;t), the multipath components corresponding to the Doppler shift f_n have phase separation $\Delta\phi_n=2\pi\ \Delta f\ \tau_n$. As Δf increases, these phase shifts result in decreased correlation between fading responses associated with two frequencies [10]. The *coherence bandwidth* $(\Delta f)_c$ provides a measure of this correlation. If the frequency separation is less than $(\Delta f)_c$, the signals C(f;t) and C(f+Δf;t) are strongly correlated, and thus fade similarly. The coherence bandwidth is inversely proportional to the multipath spread. However, the exact relationship between the coherence bandwidth and the multipath spread depends on the underlying meaning of the strong correlation of fading signals at different frequencies and varies depending on the channel model [2,3]. For example, if $|\phi_c(\Delta f)|$ is required to remain above 0.9, the corresponding coherence bandwidth is defined as $(\Delta f)_c \approx 1/\ (50\ \sigma_\tau)$ where σ_τ is the rms delay spread. When the frequency correlation is allowed to decrease to 0.5, greater coherence bandwidth $(\Delta f)_c \approx 1/\ (5\ \sigma_\tau)$ results.

The time variation of the channel response $c(\tau, t)$ due to the Doppler shift can be statistically characterized using the *spaced-time correlation function* determined from (9) as

$$\phi_c(0;\Delta t) \equiv \phi_c(\Delta t) \tag{10}$$

or its Fourier transform $S_c(\lambda)$ [1]. The function $S_c(\lambda)$ is called the *Doppler power spectrum* of the channel. As the maximum Doppler shift increases, the channel variation becomes more rapid (see (4)), and $S_c(\lambda)$ widens, resulting in *spectral broadening* at the receiver. The shape of the autocorrelation function depends on channel characteristics. For example, the popular Rayleigh fading channel discussed in section 4 has the autocorrelation function

$$\phi_c(\Delta t) = J_0\ (2\ \pi\ f_{dm}\ \Delta t), \tag{11}$$

where $J_0(.)$ is the zero-order Bessel function of the first kind [11]. The Doppler power spectrum for this channel is given by:

$$S_c(\lambda)=1/(\pi f_{dm})\ [1-(f/f_{dm})^2]^{1/2},\ |f| \le f_{dm}. \qquad (12)$$

These functions are plotted in Figure 6.

Time variation of the fading channel is characterized in terms of the *Doppler spread* and the *coherence time*. The Doppler spread B_d is defined as the range of frequencies over which the Doppler power spectrum is essentially nonzero. For example, in (12), $B_d=2f_{dm}$. The coherence time $(\Delta t)_c$ measures the time interval over which the time variation is not significant, or the samples of the fading signal are strongly correlated when their time separation is less than the coherence time, although different interpretations are used [3]. The Doppler spread and the coherence time are inversely proportional to one another. A popular rule of thumb is $(\Delta t)_c=0.423/f_{dm}$. This definition implies that if the time separation is greater than the coherence time, the signals will be affected differently by the channel.

Relationship between Signal Characteristics and the Fading Channel Model

Consider a linear communication system that transmits data at the symbol rate 1/T and employs a pulse shape with the complex envelope $s_l(t)$ and the frequency response $S_l(f)$ [1]. Assume the bandwidth W of the transmitted signal is approximately 1/T. The resulting output signal is characterized in terms of the response of the channel to this pulse shape as in (6), and the frequency response of the output signal is given by $C(f;t)\ S_l(f)$. The relationship between the symbol interval (or bandwidth W) and the statistical fading channel parameters defined above dictate the choice of the underlying channel model used in analyzing performance of wireless communication systems.

First, consider the *multipath channel characterization* and *signal dispersion*. Suppose the symbol interval is much larger than the multipath spread of the channel, $T >> T_m$. Then all multipath components arrive at the receiver within a small fraction of the

symbol interval. In this case, the coherence bandwidth significantly exceeds the bandwidth of the signal, $W << (\Delta f)_c$. Thus, all spectral components are affected by the channel similarly. Also, there is no *multipath-induced intersymbol interference* (ISI) in this case. This channel is modeled as complex time-varying attenuation c(t) (4) (also given by C(0;t)), so the complex envelope of the received signal is $r(t)=c(t)\ s_l(t)$. It is called *frequency-nonselective*, or *flat fading* channel. These channels primarily occur in *narrowband* transmission systems.

If the symbol interval is smaller the multipath spread of the channel, $T < T_m$, or equivalently, the coherence bandwidth is smaller than the signal bandwidth, $W > (\Delta f)_c$, the channel becomes *frequency selective* (also sometimes called multipath fading channel). A common rule of thumb is that the channel is frequency selective if $T<10\sigma_\tau$, and flat fading if if $T\geq 10\sigma_\tau$, where σ_τ is the rms delay spread [3]. With this definition of a frequency selective channel, spectral components of the transmitted signal separated by the coherence bandwidth fade differently, resulting in frequency diversity, as discussed in Section 5. On the other hand, frequency selectivity also causes dispersion, or ISI, since delayed versions of the transmitted signal arrive at the receiver much later (relative to the symbol interval) than components associated with small delays. This channel is often modeled using several fading rays with different excess multipath delays

$$c(t) = c_1(t)\ \delta(t-\tau_1) + c_2(t)\ \delta(t-\tau_2) + \ldots\ c_L(t)\ \delta(t-\tau_L), \qquad (13)$$

where the components $c_l(t)$, $l=1,\ldots,L$ are uncorrelated flat fading (e.g Rayleigh distributed) random variables. The powers associated with these rays are determined by the multipath intensity profile (8).

Now, consider *rapidity*, or *time variation* of the fading channel. The channel is considered *slowly varying* if the channel response changes much slower than the symbol rate. In this case, the symbol interval is much smaller than the coherence time, $T << (\Delta t)_c$, or the signal bandwidth significantly exceeds the Doppler spread, $W >> B_d$. If the

symbol interval is comparable to or greater than the coherence time, (or the coherence bandwidth is similar to or exceeds the signal bandwidth), the channel is *fast fading*. While most mobile radio, or PCS, channels are slowly fading, as the velocity of the mobile and the carrier frequency increase, the channel becomes *rapidly time-varying* since the Doppler shift increases (see (5)). This rapid time variation results in time selectivity (which can be exploited as time diversity), but degrades reliability of detection and channel estimation [12-14].

4. Fading Channel Models

The *complex Gaussian distribution* is often used to model the equivalent lowpass flat fading channel. This model is justified since superposition of many scattered components approximates a Gaussian distribution by the Central Limit Theorem. Even if the number of components in (5) is modest, experiments show that the Gaussian model is often appropriate. The *Rayleigh fading* process models fading channels without strong *Line of Sight (LOS)*. Define $c(t) = c_I(t) + jc_Q(t)$, where the in-phase (real) and quadrature (imaginary) components are independent and identically distributed (i.i.d.) zero-mean stationary real Gaussian processes with variances σ^2. The average power of this process is $1/2\ E[c^*(t)\ c(t)] = \sigma^2$. The amplitude of this process has a Rayleigh distribution with the probability density function (pdf):

$$p_R(r) = \frac{r}{\sigma^2} \exp(-\frac{r^2}{2\sigma^2}), \tag{14}$$

and the phase is uniformly distributed:

$$p_\Theta(\theta) = \frac{1}{2\pi} \quad |\theta| \le \pi \tag{15}$$

The Rayleigh distribution is a special case of the *Nakagami-m* distribution that provides a more flexible model of the statistics of the fading channel. The pdf of the amplitude of the Nakagami-m distribution is [1]

$$p_R(r) = 2/\Gamma(m)\,(m/\Omega)^m\, r^{2m-1} \exp(-m r^2/\Omega), \quad (16)$$

where $\Gamma(.)$ is the Gamma function[11], $\Omega=E(R^2)$ and the parameter m is the fading figure given by $m = \Omega^2/E[(R^2-\Omega)^2]$, $m \geq 1/2$ While the Rayleigh distribution uses a single parameter $E(R^2) = 2\sigma^2$ to match the fading statistics, the Nacagami-m distribution depends on two parameters, $E(R^2)$ and m. For m=1, the density (16) reduces to Rayleigh distribution. For $1/2 \leq m < 1$, the tail of the Nakagami-m pdf decays slower than for Rayleigh fading, whereas for m>1, the decay is faster. As a result, the Nakagami-m distribution can model fading conditions that are either more or less severe than Rayleigh fading. The Nakagami-m pdf for different values of m is illustrated in Figure 7.

The Rayleigh distribution models a complex fading channel with zero mean that is appropriate for channels without the line-of-sight (LOS) propagation. When strong non-fading, or specular components, such as LOS propagation paths, are present, a dc component needs to be added to random multipath, resulting in *Ricean* distribution. The pdf of the amplitude of Ricean fading is given by

$$p_R(r) = (r/\sigma^2) \exp - [(r^2+s^2)/2\sigma^2]\, I_0(rs/\sigma^2), \quad r \geq 0 \quad (17)$$

where s is the peak amplitude of the dominant nonfading component and $I_0(.)$ is the modified Bessel function of the first kind and zero-order [11]. The *Ricean factor* K specifies the ratio of the deterministic signal power and the variance of the multipath:

$$K = 10 \log_{10}(s^2/2\sigma^2)\ (dB) \quad (18)$$

As $s \rightarrow 0$ ($K \rightarrow -\infty$), the power of the dominant path diminishes, and the Rician pdf converges to the Rayleigh pdf. Examples of Rician fading and other LOS channels include airplane to ground communication links and microwave radio channels [1].

As an alternative to modeling the Rayleigh fading as a complex Gaussian process, one can instead approximate the channel by summing a set of complex sinusoids as in (4). The number of sinusoids in the set must be large enough so that the pdf of the resulting envelope provides an accurate approximation to the Rayleigh pdf. The Jakes

model is a popular simulation method based on this principle [10]. The signal generated by the model is:

$$c(t) = \sqrt{\frac{2}{N}} \sum_{n=1}^{N} e^{j(\omega_d t \cos\alpha_n + \phi_n)}, \tag{19}$$

where N is the total number of plane waves arriving at uniformly spaced angles α_n as shown in Figure 8. The c(t) can be further represented as:

$$c(t) = \frac{E_0}{\sqrt{2N_0 + 1}} (c_I(t) + jc_Q(t))$$

$$c_I(t) = 2\sum_{n=1}^{N_0} \cos\phi_n \cos\omega_n t + \sqrt{2}\cos\phi_N \cos\omega_m t$$

$$c_Q(t) = 2\sum_{n=1}^{N_0} \sin\phi_n \cos\omega_n t + \sqrt{2}\sin\phi_N \cos\omega_m t$$

where $N_0 = \frac{1}{2}(\frac{N}{2} - 1)$, $\omega_m = 2\pi f_{dm}$ and $\omega_n = \omega_m \cos(\frac{2\pi n}{N})$. The parameter N_0+1 is often referred as the number of oscillators in the Jakes model, and N is termed as the number of scatterers. The Jakes model with as few as nine oscillators (N_0 = 8, and N = 34) closely approximates the Rayleigh fading distribution (14,15).

When a multipath fading channel with impulse response (13) needs to be modeled, the Jakes model can be extended to produce several uncorrelated fading components using the same set of oscillators [10]. The autocorrelation function and the Doppler spectrum of the signals generated by the Jakes model are characterized by equations (11) and (12), respectively, and are shown in Figure 6. This statistical characterization is appropriate for many channels where the reflectors are distributed uniformly around the mobile (*isotropic* scattering). Several other approaches to simulating Rayleigh fading channels based on *Clarke and Gans fading models* are described in [3]. Moreover, *physical models* are useful (e.g., when the variation of amplitudes, frequencies and phases in (4) is important to model as in *long-range fading prediction*) and *autoregressive (Gauss-Markov)* models are often utilized to approximate

fading statistics in fading estimation algorithms since they result in rational spectral characterization [12,13].

5. Diversity Techniques and Performance Analysis

Performance Analysis for Flat Fading Channels

Fading channels undergo dramatic changes in received power due to multipath and Doppler effects. When communication signals are transmitted over these channels, the bit error rate (BER) varies as a function of the signal-to-noise ratio and is significantly degraded relative to the BER for the additive white Gaussian noise (AWGN) channel with the same average signal-to-noise ratio. Consider the following example of transmission of Binary Phase Shift Keyed (BPSK) signal over the flat Rayleigh fading channel. At the output of the matched filter and sampler at the bit rate $1/T_b$ (where T_b is the bit interval), the complex envelope of the received signal is

$$r_k = c_k\, b_k + z_k, \tag{20}$$

where c_k are the samples of the fading signal c(t), b_k is the i.i.d. information sequence that takes on values {+1, -1}, and z_k is the i.i.d. complex white Gaussian noise sequence with the variance $1/2\ E[|z_k|^2]=N_0$. Since the channel is assumed to be stationary, we omit the subscript k in subsequent derivations. The equivalent passband energy is normalized as $E_b = 1/2$, so the instantaneous Signal-to-Noise ratio (SNR) at the receiver is given by

$$\gamma = |c|^2 / 2N_0, \tag{21}$$

Assume without loss of generality that the average power of the fading signal $E[|c_k|^2]=1$. Then the average SNR per bit

$$\Gamma = 1/ 2N_0, \tag{22}$$

Suppose coherent detection of the BPSK signal is performed, and signal phase is estimated perfectly at the receiver. (This assumption is difficult to satisfy in practice for rapidly varying fading channels [12,13], so the analysis below represents a lower bound on the achievable performance.) The BER for each value of the instantaneous SNR (21) can be computed from the BER expression for the AWGN channel [1]:

$$\text{BER}(\gamma) = Q[(2\gamma)^{1/2}], \tag{23}$$

where the Q-function $Q(x) = 1/(2\pi)^{1/2} \int_{-\infty}^{x} \exp(-y^2/2)\, dy$. To evaluate average BER for the Rayleigh fading channel, the BER (23) has to be averaged over the distribution of the instantaneous SNR:

$$\text{BER} = \int_{0}^{\infty} Q[(2\gamma)^{1/2}]\, p(\gamma)\, d\gamma . \tag{24}$$

Since $|c|$ is Rayleigh distributed, the instantaneous SNR γ has a chi-square distribution with the pdf $p(\gamma) = 1/\Gamma \exp(-\gamma/\Gamma)$, $\gamma \geq 0$. When this density is substituted in (24), the resulting BER for binary BPSK over flat Rayleigh fading channel is:

$$\text{BER} = 1/2\,[1-(\Gamma/(1+\Gamma))^{1/2}]. \tag{25}$$

The BER for other fading distributions (e.g. Rician or Nakagami-m) can be obtained similarly by averaging the BER for AWGN (23) over the fading statistics as in (24). Figure 9 illustrates performance of BPSK over a Nakagami-m fading channel for different values of m. Observe that as m increases, the fading becomes less severe, and the BER approaches that of the AWGN channel. Rayleigh fading (m=1) results in significant SNR loss relative to the non-fading channel. In fact, for large SNR, the BER in (25) behaves asymptotically as $1/4\,\Gamma$, whereas the BER decreases exponentially with

SNR for AWGN. The error rates of other modulation methods (e.g. coherent and noncoherent Frequency Shift Keying (FSK), Differential PSK (DPSK)) also *decrease only inversely with SNR*, causing very large power consumption.

Diversity Techniques

The poor performance of flat fading channels is due to the presence of deep fades in the received signal (Figure 4) when the received SNR is much lower than the average SNR value. *Diversity techniques* help to combat fading by sending replicas of transmitted data over several uncorrelated (or partially correlated) fading channels. Since it is unlikely that these channels will go through a deep fade at the same time, higher average received SNR results when the outputs of the diversity branches are combined. Many diversity techniques are used in practice.

In *space,* or *antenna diversity* systems, several antenna elements are placed at the transmitter and/or receiver and separated sufficiently far apart to achieve desired degree of independence. (Note that the correlation function in space is analogous to that in time [10]. Typically, antenna separation of about $\lambda/2$ at the mobile and several λ at the base station are required to achieve significant antenna decorrelation, where λ is the wavelength.)

Time diversity relies on transmitting the same information in several time slots that are separated by the coherence time $(\Delta t)_c$. Time diversity is utilized in coded systems by interleaving the outputs of the encoder.

Frequency diversity can be employed when the transmitter bandwidth is larger than the coherence bandwidth of the channel, and several fully or partially uncorrelated fading components can be resolved. The number of such uncorrelated components is

determined by the ratio $W/(\Delta f)_c$ [1]. In PSK or Quadrature Amplitude Modulated (QAM) systems, the transmitter bandwidth is approximately 1/T. Due to narrow tranmission bandwidth, these channels are often frequency nonselective. When frequency selectivity is present, it usually causes ISI since the multipath delay is significant relative to the symbol interval. Thus, *equalizers* are used to mitigate the ISI and to obtain the diversity benefit [1,12-14]. On the other hand, *Direct Sequence Spread Spectrum* systems (DSSS) employ waveforms with the transmission bandwidth that is much larger than the symbol rate 1/T, and thus enjoy significant frequency diversity. DSSS signals are designed to achieve approximate orthogonality of multipath-induced components, thus eliminating the need for equalizers. Frequency diversity combining in these systems is achieved using a *RAKE correlator* [1].

In addition to the diversity techniques mentioned above, *angle-of-arrival* and *polarization* diversity are utilized in practice. Different diversity methods are often combined to maximize diversity gain at the receiver. To illustrate the effect of diversity on the performance of communication systems in fading channels, consider the following simple example. Suppose the transmitted BPSK symbol b_k is sent over L independent Rayleigh fading channels (we suppress the time index k below). The received equivalent lowpass samples are:

$$r^i = c^i b + z^i, \quad i=1,\ldots,L, \tag{26}$$

where c^i are i.i.d. complex Gaussian random variables with variances $E[|c^i|^2] = 1/L$ (this scaling allows us to compare performance directly with a system without diversity in (20)), b is the BPSK symbol as in equation (20), and z^i are i.i.d. complex Gaussian noise

samples with 1/2 $E[|z_k|^2]=N_0$. Thus, the average SNR *per channel* (*diversity branch*) is $\Gamma_c = \Gamma/L$, where Γ is the SNR per bit.

There are several options for combining L diversity branches. For example, the branch with the highest instantaneous SNR can be chosen resulting in *selection diversity*. Alternatively, *equal gain combining* is a technique where all branches are weighted equally and co-phased [3]. The maximum diversity benefit is obtained using the *Maximum Ratio Combining* (MRC) (this is also the most complex method). In MRC, the outputs r^i are weighted by the corresponding channel gains, co-phased and summed producing the decision variable (the input to the BPSK threshold detector) :

$$U = (c^1)^* r^1 + (c^2)^* r^2 + \ldots + (c^L)^* r^L,$$

Note that if a signal undergoes a deep fade, it carries weaker weight than a stronger signal with higher instantaneous power. It can be shown that for large SNR, the BER for this method is approximately [1]:

$$BER \approx (1/(4\,\Gamma_c))^L \binom{2L-1}{L}. \qquad (27)$$

This BER of MRC for BPSK is illustrated in Figure 10 for different values of L (binary PSK curve). The figure also shows performance of two less complex combining methods used with orthogonal FSK (*square law combining*) and DPSK. The latter two techniques are noncoherent (do not require amplitude or phase estimation.) From equation (27) and Figure 10 we observe that the *BER for all methods decreases inversely with the L^{th} power of the SNR*. Thus, diversity significantly reduces power consumption in fading channels.

In addition to diversity, *adaptive transmission* is an effective tool in overcoming the effects of fading. The idea is to adjust the transmitted signal (power, rate, etc) to fading conditions to optimize average power and bandwidth requirements. Many recent

advances in the area of communication over fading channels and additional references are presented in [12,13].

6. Summary

The fading signal was characterized in terms of large-scale and small-scale fading. The large-scale fading models that describe the average and statistical variation of the received signal power were presented. The small-scale fading channel was characterized statistically in terms of its time-variant impulse response. Time and frequency domain interpretation was provided to describe signal dispersion and fading rapidity, and it was shown how the transmitted signal effects the choice of fading channel model. Several statistical models of fading channels were presented, and simulation techniques were discussed. Finally, performance limitations of fading channels were revealed, and fading mitigation methods using diversity techniques were reviewed.

Acknowledgement

The author is thankful to Shengquan Hu, Hans Hallen, Tung-Sheng Yang, Ming Lei, Jan-Eric Berg and Henrik Asplund for their assistance and helpful comments. This work was partially supported by NSF grant CCR-9815002 and ARO grant DAA19-01-1-0638.

References

[1] J. G. Proakis, *Digital Communications*. Fourth Edition, McGraw-Hill, 2001.

[2] B. Sklar, "Rayleigh Fading Channels in Mobile Digital Communication Systems, Part 1: Characterization," *IEEE Commun. Mag.*, Vol. 35, No. 7, July 1997, pp. 90 – 100.

[3] T. S. Rappaport, *Wireless Communications: Principles and Practice,* 2nd edition, Prentice-Hall, 2002.

[4] H. L. Bertoni, *Radio Propagation for Modern Wireless Systems*, Prentice Hall, 2000.

[5] W. C. Y. Lee, *Mobile Communications Engineering: Theory and Applications*, 2nd edition, McGraw-Hill Telecommunications,1997.

[6] R. Steele, *MobileRadio Communications*, Pentech Press, 1992.

[7] G. L. Stuber, *Principles of Mobile Communication*, Kluwer Academic Publishers, 2001.

[8] P. A. Bello, "Characterization of Randomly Time-Variant Linear Channels," *IEEE Trans. Commun. Systems*, Vol. 11, pp. 360-393, 1963.

[9] S. Stein, "Fading Channel Issues in System Engineering," *IEEE J. Select. Areas. Commun.*, Vol. 5, No. 2, Feb. 1987, pp. 68 - 69.

[10] W. C. Jakes, *Microwave Mobile Communications*. Wiley, New York, 1974.

[11] M. Abramowitz and I. A. Stegun, *Handbook of Mathematical Functions*, National Bureau of Standards, 1981.

[12] E. Biglieri, J. Proakis, S. Shamai (Shitz), " Fading Channels: Information-Theoretic and Communications Aspects," *IEEE Transactions on Information Theory*, Vol. 44, No. 6, Oct. 1998, pp. 2619-2692.

[13] *IEEE Signal Processing Magazine*, Special Issue on Advances in Wireless and Mobile Communications, G. B. Giannakis, Guest Editor, Vol. 17, No.3, May 2000.

[14] B. Sklar, "Rayleigh Fading Channels in Mobile Digital Communication Systems, Part 2: Mitigation," *IEEE Commun. Mag.*, Vol. 35, No. 7, July 1997, pp. 102 – 109.

[15] Seidel, S.Y., Rappaport, T. S., Jain, S., Lord, M., and Singh, R., "Path Loss, Scattering, and Multipath Delay Statistics in Four European Cities for Digital Cellular and Microcellular Radiotelephone," *IEEE Transactions on Vehicular Technology*, Vol. 40, No. 4, pp. 721-730, Nov. 1991.

[16] Rappaport, T. S., Seidel, S.Y. and Singh, R., "900MHz Multipath Propagation Measurements for U.S. Digital Cellular Radiotelephone," *IEEE Transactions on Vehicular Technology*, pp. 132-139, May 1990.

[17] Miyagaki, Y., Morinaga, N., and Namekawa, T., "Error Probability Characteristics for CPFSK Signal through m-Distributed Fading Channel," *IEEE Trans. Commun.*, vol. COM-26, pp. 88-100, Jan. 1978.

Permission has been requested for all figures reprinted from other sources.

Captions for these figures are the same as in the source. Copies of these figures are provided with the hard copy of the manuscript.

Figure 1. Reprinted from [2].

Figure 2. Reprinted from [15]

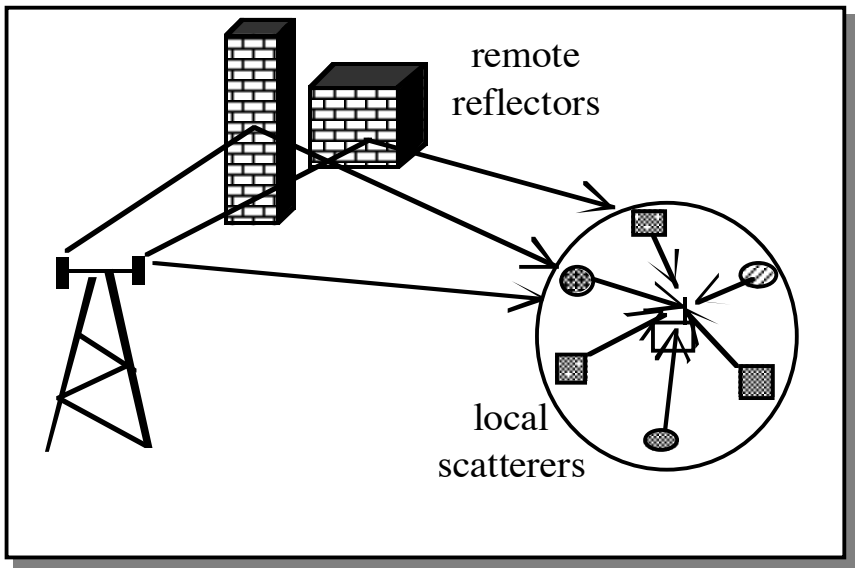

Figure 3. Typical Mobile Radio Environment

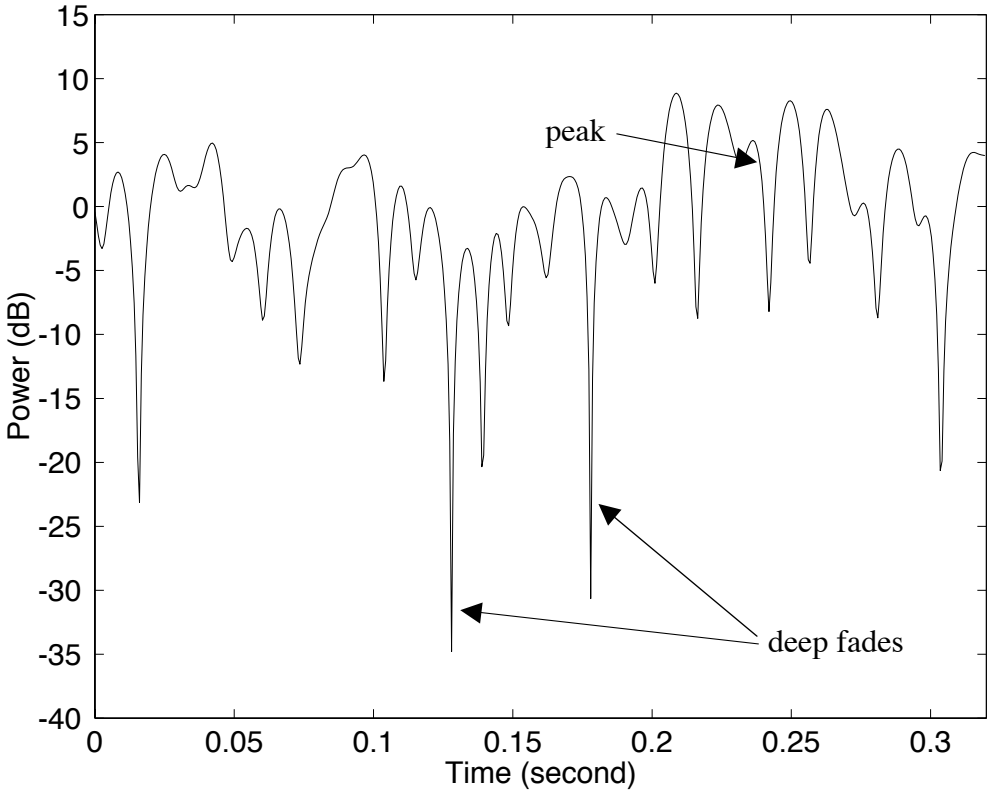

Figure 4. A typical fading signal (Provided by Ericsson Inc.)

Figure 5. Reprinted from [16].

(a)

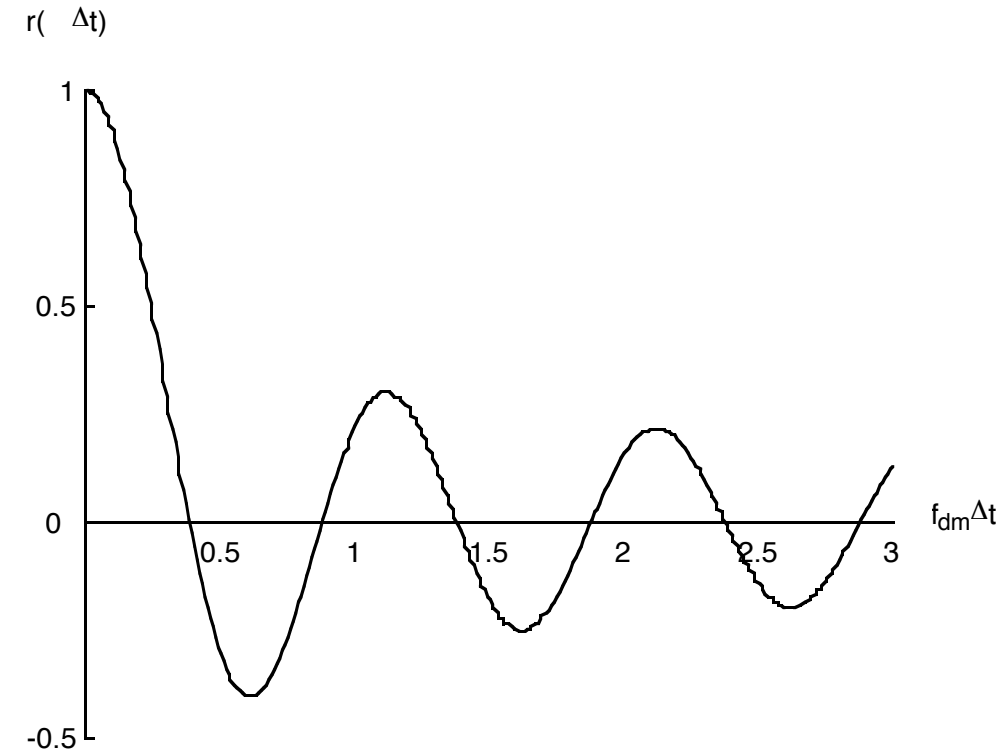

(b)

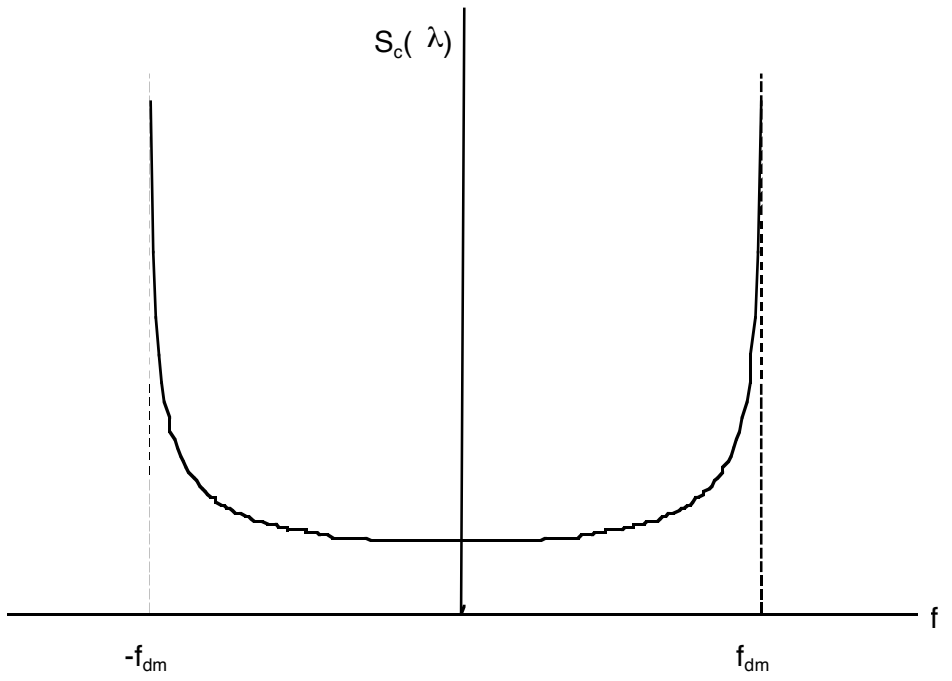

Figure 6 (a) The spaced-time autocorrelation function of the Rayleigh fading channel
(b) The Doppler power spectrum of the Rayleigh fading channel

Figure 7**.** Reprinted from [17].

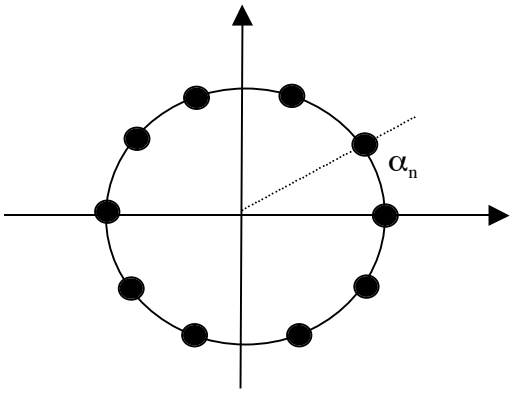

Figure 8. The Jakes' model with N=10 scatterers (N_0 = 2, 3 oscillators).

Figure 9. Reprinted from [1].

Figure 10. Reprinted from [1].